Mecánica Computacional Vol. XXIV
A. Larreteguy (Editor)
Buenos Aires, Argentina, Noviembre 2005

# FLOW AROUND A SHARP-EDGED SURFACE-MOUNTED CUBE BY LARGE EDDY SIMULATION

**Norberto Nigro*, Germán Filippini*, Gerardo Franck *, Mario Storti*and Jorge D'Elía***

*Centro Internacional de Métodos Computacionales en Ingeniería (CIMEC)
Instituto de Desarrollo Tecnológico para la Industria Química (INTEC)
Universidad Nacional del Litoral - CONICET
Parque Tecnológico Litoral Centro (PTLC) s/n, 3000-Santa Fe, Argentina
e-mail: gfilippini@ceride.gov.ar, (nnigro,mstorti,jdelia)@intec.unl.edu.ar
web page: http://venus.ceride.gov.ar/CIMEC

**Key Words:** bluff bodies, wake flow, turbulence, large eddy simulation, finite elements, parallel computing, fluid mechanics

**Abstract.**

*Unsteady separated flows around bluff bodies such as cubes, rectangular and circular cylinders and flat plates are relevant to many engineering designs. For numerical validations, some test cases have been chosen as benchmarks in the turbulence modeling community where several numerical methods, Sub-Grid Stress (SGS) models and mesh resolutions are currently validated, see paper by Kogaki[1]*

*We have performed Large Eddy Simulations of the three dimensional flow field around a wall-mounted cube, a very popular benchmark. In this case, experiments show a fully turbulent flow regime everywhere and displays no obvious regularity or periodicity and contains many coherent structures both downstream and upstream. The selected flow conditions for the present numerical simulations are taken from those suggested by Rodi.[2] The Reynolds number is 40,000 while the boundary conditions include a fully developed channel flow at inlet, periodic at lateral sides, null pressure at outlet and no-slip at the wall surface. Here, the upstream flow at inlet is a fully developed channel flow which is obtained by a previous running for such case. Flow visualization is used to clarify the flow behavior.*

## 1 INTRODUCTION

The goal of this work is to validate the LES implementation carried out on the *Petsc-Fem* code developed at *CIMEC*.[3,4] With this target at hand it is possible to identify the limits of validity of such a model, understanding the reasons for these limits. Towards this objective two cases were proposed: a square cylinder (case A) and a wall-mounted cube (case B), as denoted by Rodi et al.[2] Both benchmarks are oriented to the flow around bluff-bodies, and they are suitable to explore the feasibility of the LES to relate engineering problems because they show complicated flow events such as massive separations, impinging, transition to turbulence and formation of vortex streets. These flow patterns are commonly found in the aerodynamic analysis of ground vehicles, specially cars,[5,6] area of interest at CIMEC.[7,8]

While the first test is part of another paper[9] the second example is treated in detail here, in the next sections.

So far the hardware and software has grown nowadays that parallel computation used in turbulence modeling makes LES not only feasible but also a very promising model to attain a more direct vision about the flow behavior. Resolving the larger scales and modeling the smaller ones puts the limit in terms of computational resources and the complexity of the problem at hand.

The LES model used in this work is one of the simplest and due to Smagorinsky.[10] This model have several critics, one of them concerns with the usage of certain universal constant arisen from the assumption of equilibrium hypothesis, normally not found in real applications. Germano[11] proposed the usage of a dynamic coefficient variable with the local flow pattern. This modification tends to improve the model accuracy but also it makes the numerical technique more unstable. Currently a lot of work is being done in order to reduce the critics about using LES as a turbulence model instead of RANS models. Some authors put the modeling in terms of some mixing between LES and RANS, resolving the larger scales, modeling the smaller ones and doing some sort of averaging for the interactions between the smaller scales introducing one equation model for the turbulent kinetic energy of only the smaller scales.[12] Using LES it is possible to do some statistics with the flow simulation. This a posteriori task may be used as a solution quality control for further refinements, specially in mesh size distribution.

This work is exploratory in the sense that after the CFD+LES validation it follows with certain identification of the main drawbacks of this turbulence model in order to propose new ideas about how to improve it.

An important detail taken into account in this work was the evaluation of the incidence of turbulence level coming at the upstream boundary of the domain. This is one of the key problems in LES simulation and it can be solved by different ways. The simplest is to assume a spatially variable turbulent velocity profile but constant in time. A further refinement to this strategy may be using a synthetic velocity profile computed as the solution of the Orr-Sommerfeld equations for the time and the transverse spatial coordi-

nate Fourier transform. These 1D equations in the vertical direction, one for each time frequency involved and one for each transverse wave number may be solved numerically and the velocity profile is finally composed. In general a frequency bandwidth is chosen according to the most energetic scales[13]

Another way to compute the inlet velocity profile may be solving the fluid flow in the upstream channel that intersects with the cube region at its entrance boundary. For this channel flow, periodic boundary condition between inlet and outlet are normally used with a body force to balance the wall friction forces, getting at the outlet section a turbulent developed velocity profile

In this work the last mentioned strategy was adopted, with details about this extra simulation included in a section of this paper.

This paper is organized as follows: first, a physical and geometrical description of the problem is presented, followed by some numerical details taken into account and the boundary conditions adopted. The following section includes the simulation of an extra problem, the channel flow upstream the cube to compute the inlet velocity profile with a desired turbulence intensity. Some statistics are included in order to evaluate the solution obtained for this well known extra example. The following section shows the simulation results for the cube test and finally some conclusions and future work is addressed.

## 2 PHYSICAL CONFIGURATION AND NUMERICAL DETAILS

The wall-mounted cube of a channel flow has been extensively analyzed during the last years and several experimental and numerical results are available in the literature. It serves as a good benchmark for turbulence model evaluation, for CFD+LES implementation and for some parametric tuning. The physical problem of an incompressible viscous flow in turbulent regime is mathematically represented by the unsteady Navier-Stokes equations using a filter defined in such a way that the large scales motions are computed directly and the smaller ones, those that are not visible for the grid size involved, are modeled. Numerically the problem is solved using a fractional step method with finite elements. Geometric details of the problem are included in figure 1 and 2 and they were extracted from the references.[2] The fluid flow is coming through the inflow boundary condition ($x = 0$) with a bulk Reynolds number of 40,000 defined as ($Re = U_b H/\nu$), based on the bulk velocity $U_b$ and the height $H$ as the characteristic length. The unit cube is mounted at $x = x_1 = 3$ units, centered in the transverse direction $z = 0$, and rest at the channel floor $y = 0$. In the figure 1 and 2 $D = 1$, $x_2 = 6$, $z_1 = 7$ and $H = 2$ units. Even though the geometry is very simple the flow pattern is very complex with coherent structures sketched in figure 3.

The unstructured mesh employed is formed by approximately 1.3 millon of tetrahedra and 256 thousands nodes. A logarithmic velocity profile was used close to the wall with $y^+ = 1$ for the whole set of solid walls, the channel walls and the cube surface. A van-Driest factor was used to damp the turbulent viscosity close to the walls according to the proximity of the first node to the solid wall. Over the lateral boundaries ($z = \pm 3.5$)

a periodic boundary condition is imposed over the whole state vector, velocities and pressure. At the outflow, a constant pressure was imposed $p_{out} = p_{ref}$ and at the inflow, a turbulent unsteady velocity profile was used. Details about the computation of this profile are included in next sections. For the time integration a Crank-Nicolson second order scheme was used with a time step of approximately 0.05 seconds.

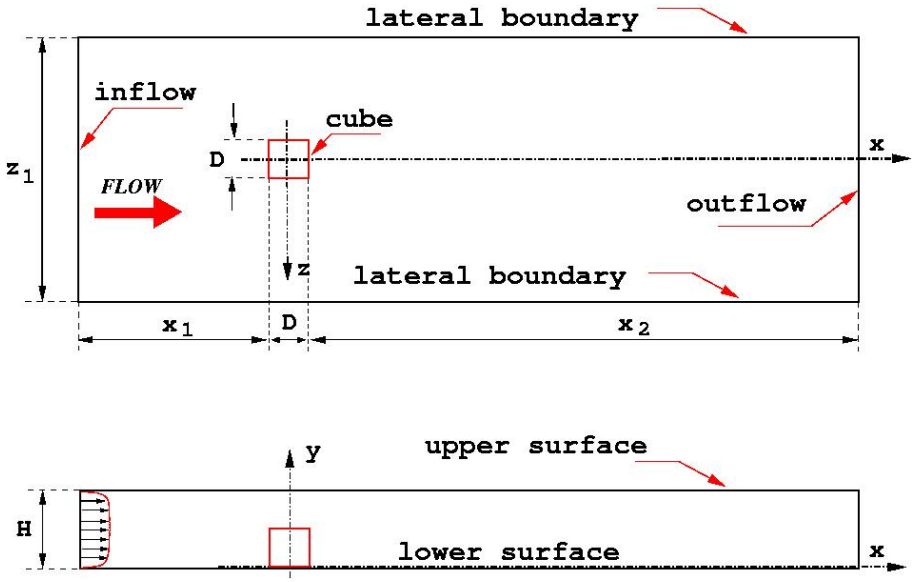


Figure 1: Geometry of a cube placed on a wind tunnel wall.

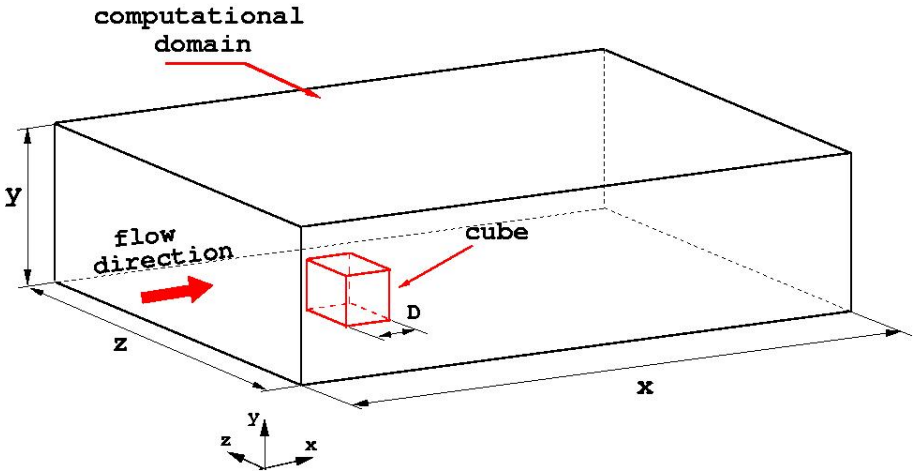


Figure 2: Perspective view of the computational domain for the cube placed on a wind tunnel wall.

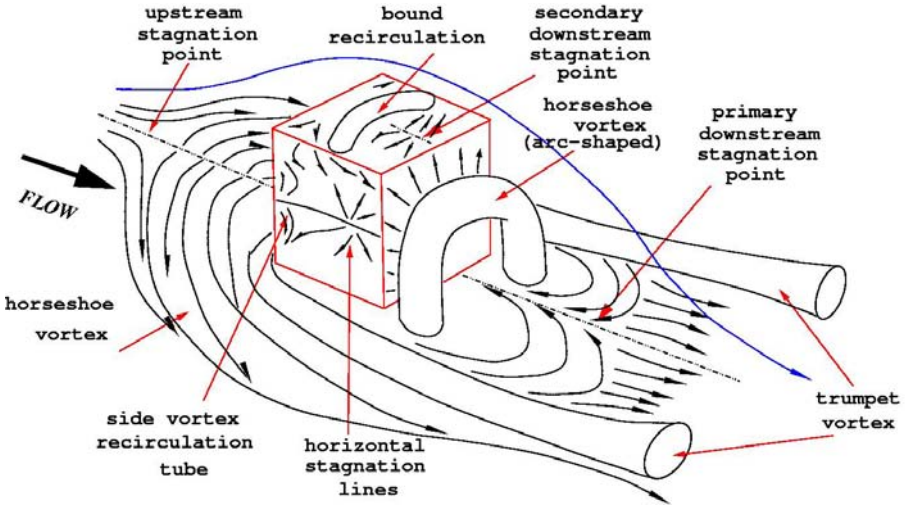


Figure 3: Schematic representation of the flow around a surface mounted cube (Hussein and Martinuzzi).

## 3 DEFINITION OF THE UPSTREAM BOUNDARY CONDITION. CHANNEL FLOW SIMULATION

The computation of the turbulence intensity of the flow coming to the section where the cube is mounted is a very difficult task to be accomplished. In order to introduce this important effect several strategies may be adopted. One simple idea used in this work is to include the region upstream to the cube section in an a priori analysis. The length of this added channel is defined to guarantee the existence of the most important length scales that may play an important role in the flow pattern around the cube. In this work a channel length of 8 units ($0 < x < 8$) was taken, keeping the same cross section of the original problem.

The mesh adopted for this extra simulation was a structured one with $50 \times 80 \times 50$ hexahedral elements in $X, Y, Z$ directions respectively. For this viscous incompressible channel flow the Navier-Stokes equations were used with the same turbulence model as for the original problem, i.e. LES-Smagorinsky, with a wall law for the computation of the shear velocity at wall using ($y^+ = 1$) and van-Driest for the atenuation of the turbulence in the presence of solid objects, like along the wall channel.

Similar spatial and temporal numerical discretizations with the original cube test were chosen, with a time step of 0.05 seconds.

For the boundary conditions, at solid walls the wall law was chosen, for entrance and outlet section a periodic boundary condition was adopted, filtering the axial scales larger than the channel length. As driven force a body force oriented with the axial direction was used and pressure was fixed in one node to remove the rigid mode.

To select the magnitude of the body force a macroscopic linear momentum balance should be done with an empirical correlation for the skin friction at the wall according to the bulk Reynolds number.[14] In this way it is possible to get the bulk Reynolds number

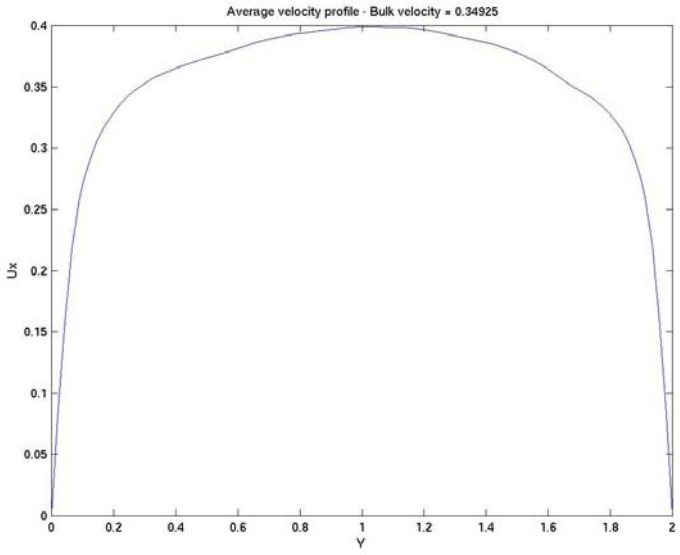


Figure 4: Mean velocity profiles at outlet section

close to the target value needed for the entrance of the flow at the cube region.

From the linear momentum balance and applying a temporal averaging assuming equilibrium it is possible to obtain the following:

$$\begin{aligned} \int_{\Omega} \rho \mathbf{g} d\Omega &= \int_{\Gamma} \tau \cdot \mathbf{n} d\Gamma \\ \rho \mathbf{g} |\Omega| &= \rho \mathbf{g} |\Gamma| H = \tau \cdot \mathbf{n} (2 \times |\Gamma|) \\ \rho \mathbf{g} H &= 2\tau \cdot \mathbf{n} \end{aligned} \tag{1}$$

where $\Omega$ is the spatial domain, $\Gamma$ is the whole boundary, in this case the channel walls, $\rho$ is the density, $\mathbf{n}$ is the unit normal at the boundary, $\mathbf{g}$ is the body force and $\tau$ is the stress tensor at wall. From (1) arises a relation between the wall traction $(\tau \cdot \mathbf{n})$ and the body force. Using the skin friction empirical correlation for channels proposed by Dean:[15]

$$\begin{aligned} C_f &= \frac{|(\tau \cdot \mathbf{n})_{\mathbf{t}}|}{\frac{1}{2}\rho {U_{bulk}}^2} \\ C_f &= 0.073 Re_b^{-0.25} \end{aligned} \tag{2}$$

where $Re_b = \rho U_{bulk} \delta / \mu$, $\delta = H/2$ is the channel half-width, $\mu = \rho\nu$ is the dynamic viscosity and $U_{bulk}$ is the bulk velocity, and $(\tau \cdot \mathbf{n})_{\mathbf{t}}$ means the tangent projection of the wall traction vector.

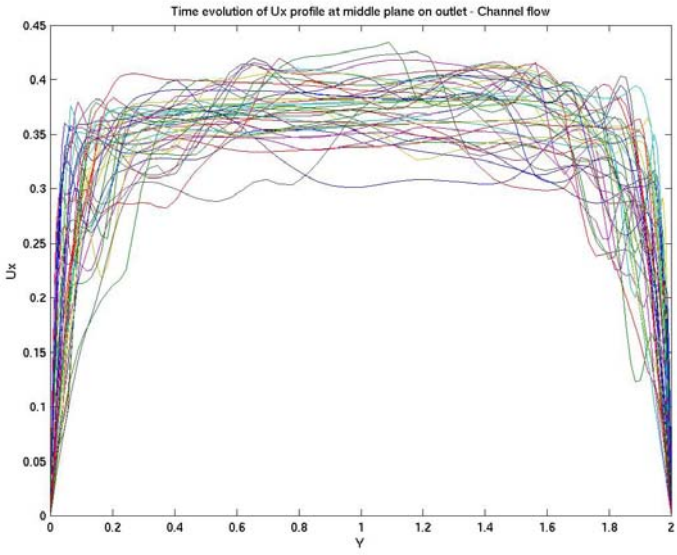


Figure 5: Instantaneous velocity profiles at middle plane outlet section

Therefore, replacing 2 in 1 follows:

$$\begin{aligned} \rho \mathbf{g} H &= 2|(\tau \cdot \mathbf{n})_{\mathbf{t}}| \\ \mathbf{g} &= \frac{2|(\tau \cdot \mathbf{n})_{\mathbf{t}}|}{\rho H} = \frac{C_f \rho {U_{bulk}}^2}{\rho H} = \frac{\rho {U_{bulk}}^2 0.073 Re_b^{-0.25}}{\rho H} \\ \mathbf{g} &= \frac{0.073 {U_{bulk}}^2 Re_b^{-0.25}}{H} \end{aligned} \tag{3}$$

with $\mathbf{g}$ in SI units.
On the other hand the friction Reynolds number is defined as:

$$Re_\tau = \frac{\rho u_\tau \delta}{\mu} = \frac{\rho \sqrt{\frac{\tau \cdot \mathbf{n}}{\rho}} \delta}{\mu} \tag{4}$$

and using 1 and 3 arises:

$$Re_\tau = \frac{\rho \sqrt{\frac{1}{2} \mathbf{g} H} \delta}{\mu} = \sqrt{\frac{0.073}{2}} Re_b^{7/8} = 0.191 \times Re_b^{7/8} \tag{5}$$

In this way it is possible to get a relation between the bulk and the friction Reynolds numbers. If the bulk Reynolds number at the entrance boundary for the cube test is $Re_b = 40000$, therefore the friction Reynolds number required is approximately $Re_\tau = 2031.5$, while the body force needed to attain this value is $\mathbf{g} = 4.1274 \times 10^{-4}$.

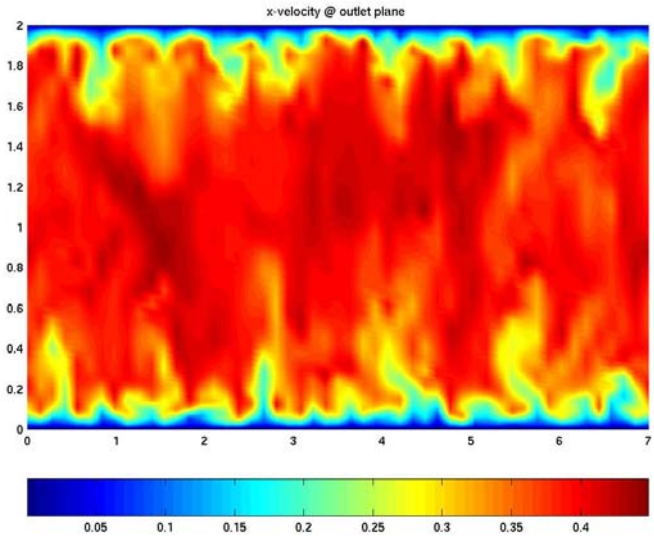


Figure 6: Instantaneous axial velocity colormap at the whole outlet section

### 3.1 Statistics analysis for the channel flow

As using LES it is possible to do some statistics with the larger scales, gaining knowledge about how large are the scales being modeled and also, as a validation tool for CFD + LES codes, because there are a lot of experimental and numerical results for channel flows.[16,17,18]

However these statistics are not necessary to define the upstream boundary condition for the cube region, coincident with the outlet boundary condition for the channel flow because all it is needed is a time evolution of the spatial distribution of the velocity at the whole inlet plane.

From the standard channel flow CFD simulation the following state function is achieved: $U(x,y,z,t) = [u_1, u_2, u_3, p](x,y,z,t)$. Taking only the states at the whole outlet boundary of the channel $U(x=8,y,z,t)$ and applying first a temporal averaging and later a $Z$ spatial averaging it is possible to get:

$$\begin{aligned} \overline{U}(x=8,y,z) &= \frac{1}{T}\int_{t_0}^{t_0+T} U(x=8,y,z,t)dt \\ \langle\overline{U}(x=8,y)\rangle &= \frac{1}{\Delta Z}\int_{-\Delta Z/2}^{\Delta Z/2} \overline{U}(x=8,y,z)dz \end{aligned} \tag{6}$$

a state that only depends on the vertical coordinate $Y$. Velocity fluctuations were computed by:

$$U'(x=8,y,z,t) = U(x=8,y,z,t) - \overline{U}(x=8,y,z) \tag{7}$$

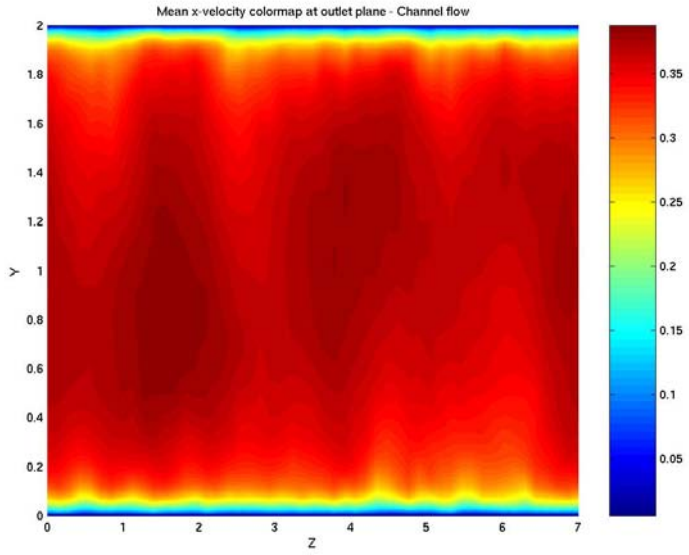


Figure 7: Mean axial velocity colormap at the whole outlet section

and using these fluctuations some measure of the turbulent kinetic energy ($k = u'_j u'_j$) and two components of the Reynolds stress tensor: $\tau_{11} = u'_1 u'_1$ y $\tau_{12} = u'_1 u'_2$ were computed. $u'_j$ is the j-component of the fluctuation velocity $u'$.

Figure 4 shows the mean velocity profile at the outlet section and the value of bulk velocity obtained while figure 5 shows the instantaneous velocity profile at the middle plane of the outlet section for different time steps. This figure shows the way in which the profile is distorted in time to produce the final mean velocity profile showed in figure 4. A colormap of the instantaneous axial velocity at the whole outlet section is shown in figure (6).

Some wrinkled patterns are concentrated at the vicinity of both walls with an approximate uniform velocity profile at the middle of the channel height. Figure 7 shows a colormap of the mean axial velocity at the whole outlet section where it is noticeable that the profile reaches an slug shape. While figure 8 shows a colormap of the instantaneous velocity fluctuation at the whole outlet section, figure 9 shows the mean turbulent kinetic energy profile at the middle plane of the outlet section. It is remarked that the peak values are placed close to the walls decreasing at the middle of the channel height approximately one order of magnitude as an evidence of the concentration of turbulence lumps around the walls. Figure 10 shows a logarithmic colormap of the mean turbulent kinetic energy at the whole outlet section where differences between regions close to the wall with those placed around the middle height one are remarked. Figures 11 and 12 show two components of the Reynolds stress tensor at the middle plane of the outlet section normalized with the square of friction velocity $u_\tau$. Finally the solution $U(x = 8, y, z, t)$ at the whole outlet boundary of the upstream channel is used as the upstream boundary condition for

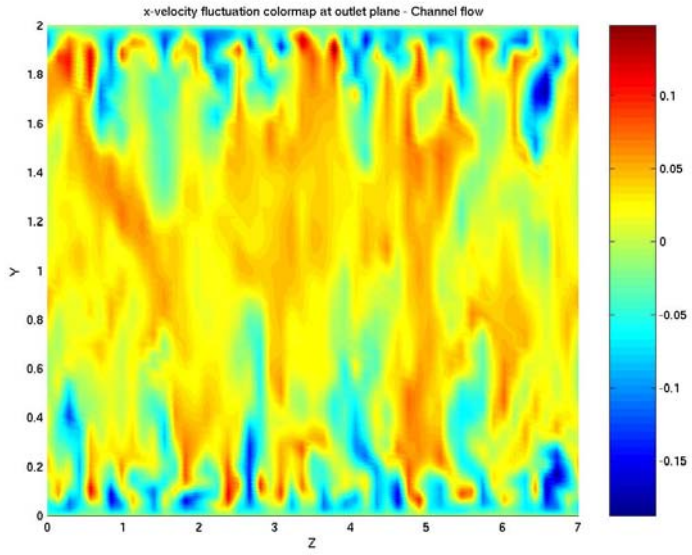


Figure 8: Instantaneous axial velocity fluctuation at the outlet section

the cube test. Because both meshes are not necessarily similar at their intersection, it is necessary some sort of interpolation: $U(x = 8, y, z, t)_{channelmesh} \rightarrow U(x = 0, y, z, t)_{cubemesh}$.

## 4 VISUALIZATION OF THE RESULTS OF HUSSEIN AND MARTINUZZI

In this section the cube test is again set up having computed the upstream boundary condition as previously explained.

Figures 13 and 14 show the experimental results obtained by Hussein and Martinuzzi in Ref.[19]. Laminar flow regime at left and turbulent regime at right give a clear image of how the fluid flow behaves in this situation. Both top views show the extension of the recirculation zone behind the cube with the flow coming from the right to the left. Both flows seem to be similar with different scales. These results serve as a setup about the flow patterns involved in the real physical world and what the simulation may capture among them. It is clear the correspondence between these figures and the sketch shown in figure 3.

## 5 VISUALIZATION OF THE NUMERICAL RESULTS

The following nomenclature will be employed in the next subsections:

1. The *particle-traces* visualize the instantaneous vector field. They can be shown as *lines* or *ribbons*;

2. The particle-trace *lines* display the path that a particle would follow if it would be

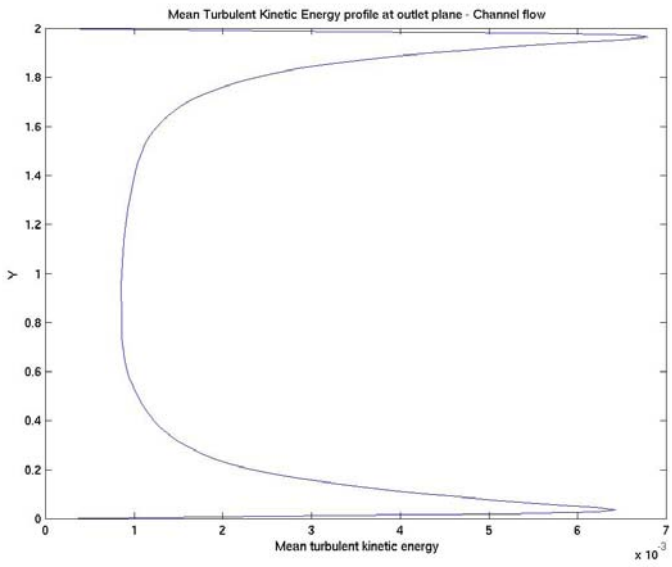


Figure 9: Mean turbulent kinetic energy profile at the middle plane of the outlet section

placed in that field. The particle can be chosen to have mass or not. The tangent of a particle-trace line is parallel to the instantaneous vector field at each point;

3. A *stream-line* is the same as a particle-trace line but for a steady-vector field or at some specified time step;

4. A *stream-ribbon* is a particle-trace line that additionally visualize the torsion of the vector field around the path of the particle. This is done through of a *ribbon* whose *width* is some user-specified value, while its *twisting* is determined by the rotation of the flow around the path of the particle;

5. A *surface-restricted* stream-line is one constrained at some cut-plane defined by the user, where only the tangential component of the vector-field is employed. Its values can be the vector magnitude (which can not be zero) or by specifying some of its components;

In the visualization software, the *particle-trace lines* and *stream-line* are computed with bar elements, while the *stream-ribbon* consist of 4-noded quadrilateral with its end-edges parallel to the $z$-axis of the global frame. Then, at each integration step of the vector field, the leading edge is rotated around the current direction of the path by the same amount that the vector field has rotated around the path.

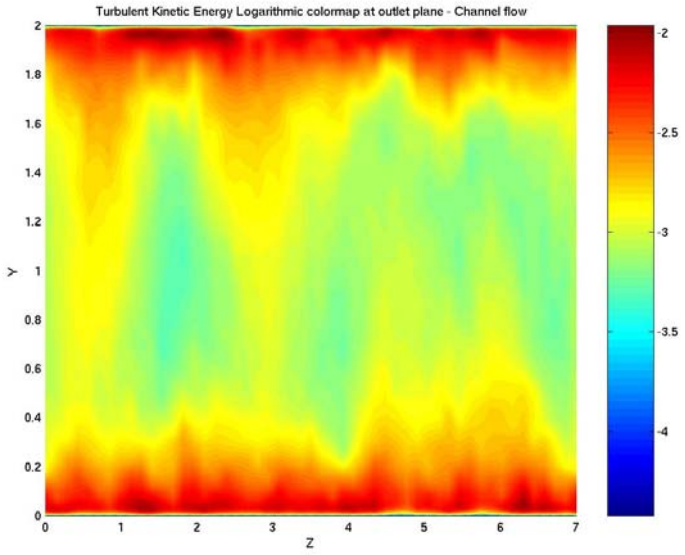


Figure 10: Mean turbulent kinetic energy colormap at the outlet section

### 5.1 Streamlines and stream-ribbons

The stream-lines and stream-ribbons are used to visualize separations and re-attachments in different places of the flow domain: front, top, bottom and lateral sides of the wind-tunnel, and behind the cube. In order to clarify the differences between the atream-lines and stream-ribbons the latter adds over the former the torsion curvature.

The instantaneous-flow behavior is compared with time-averaged one. The stream-lines are projected onto the $xz$-floor plane or near to the ground. Besides, the stream-lines are projected onto the $xy$-symmetry plane, while the trace-lines are visualized onto the body surface.

The stream-ribbons are used for visualization the flow features in the lateral and near-wakes. A better picture of the flow nature can be obtained from the time-averaged streamlines taken from some time-steps of the numerical simulations. On the other hand, iso-surfaces and contour-fills of pressure and speed are also used for identifying coherent structures and quasi-periodic sub-flows.

#### 5.1.1 At the horizontal $xz$-floor plane

It can be observed in figure 15 that the streamlines of the time-averaged flow projected onto this plane show a pair of vortices with their foci, behind the cube. There are two recirculation regions with their foci on the lateral sides of the cube. The saddle point in front of the body is followed by the horseshoe vortex.

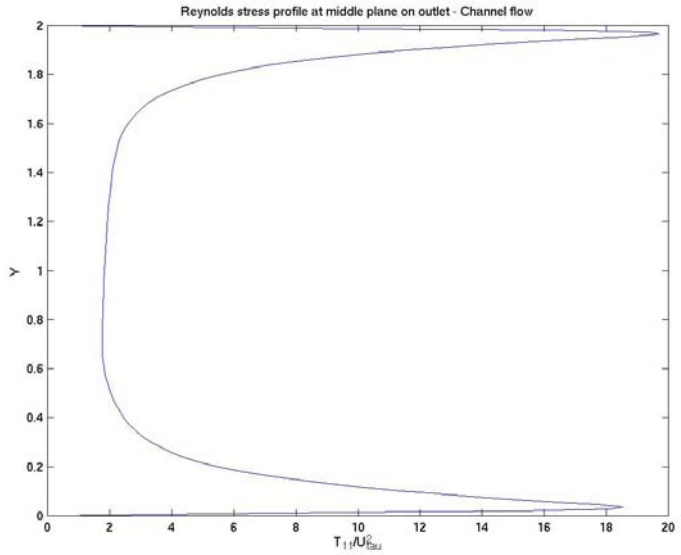


Figure 11: Reynolds stress $\frac{r_{11}}{u_\tau^2}$

### 5.1.2 At the vertical $xy$-plane ($z = 0$)

Flow separation occurs and a subsequent horseshoe vortex system is developed due to the adverse pressure gradient incurred by the obstacle.

In figure16, there is a horseshoe vortex in front of the cube and recirculation region on the top and behind the cubic obstacle.

Figure 16 shows a behavior of the horseshoe vortex in front of the cube. From this figure, it can be noted that unsteady horseshoe vortex systems can be obtained when $Re >$ 2800 according to experiment of Baker[20]. They apparently follow a quasiperiodic behavior of this horseshoe vortex system. The dependency of the quasiperiodic behavior on the type of flow is unique to horseshoe vortices in internal flow, and remains to be further explored for the purposes of not only practical applications but also basic understanding of horseshoe vortices.

Comparing figure 13 with 16 there is some differences that needs more work to be understood. For the numerical simulation there is a marked trend to extend the recirculation further than the experimental and also the flow has a stronger separation respect to the measurements. One of the possible reasons for such a behavior may be an inadequate grid size close to the cube that may induce a smaller attenuation of the turbulent viscosity by the the Van-Driest damping factor.

Figure 17 at left shows a time-average velocity magnitude with vorticity over the cube and figure 17 at right the field vorticity in the symmetry plane and the gradient velocity over the cubic obstacle.

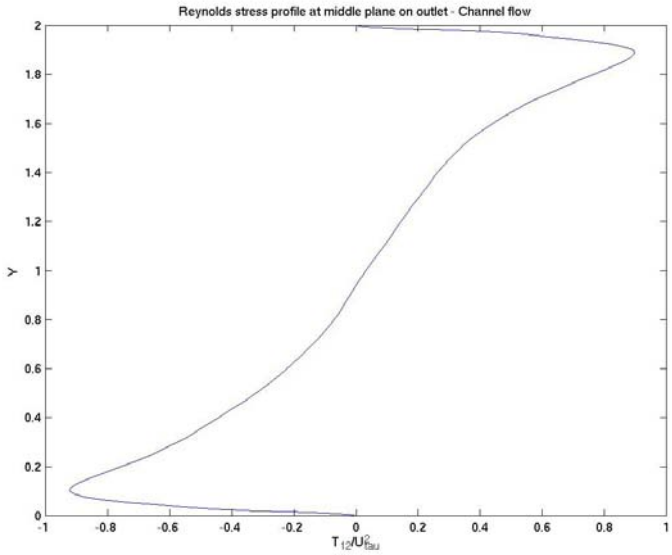


Figure 12: Reynolds stress $\frac{r_{12}}{u_\tau^2}$

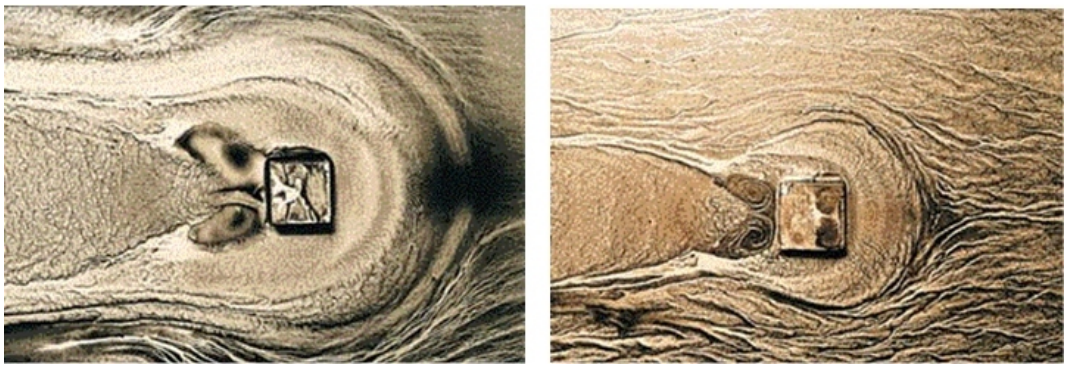

Figure 13: Experimental results of the flow around a surface mounted cube (Hussein and Martinuzzi). Left: laminar flow. Right: turbulent flow.

### 5.1.3 Stream-ribbons

In figure 18 an exchange of fluid between the separation regions can be observed. From this picture it can be concluded that the separation-region around a three-dimensional bluff-body can not be closed. In this picture it can be observed an exchange between the top surface cube to the near wake region. To support this conclusion, figure 19 shows the stream-ribbons at the lateral sides as in the near-wake behind the cube. It should be noted how the stream-ribbons stretch from the lateral to the back vortices showing a fluid exchange among these vortices.

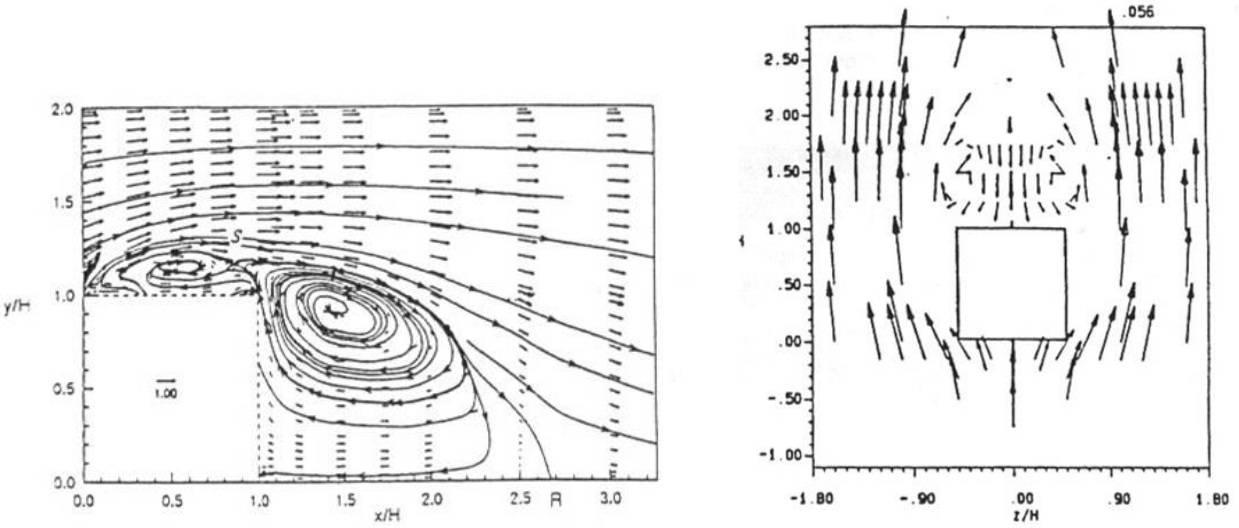


Figure 14: Experimental results of the flow around a surface mounted cube (Hussein and Martinuzzi). Left: vector field center plane. Right: vector field horizontal plane.

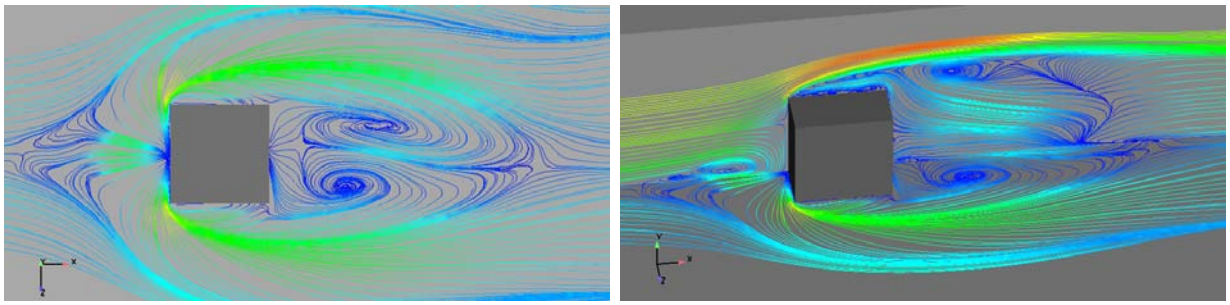

Figure 15: Trace-lines of the velocity magnitude over the floor plane ($z = 0$): averaged-flow (left) and perspective-view (right).

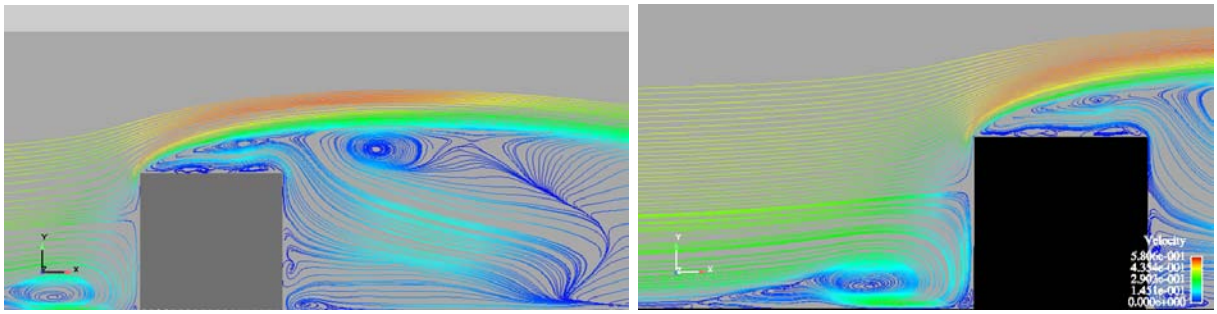

Figure 16: Streamlines of the time-averaged flow projected onto left: the center plane of the cube and right: in front of the cube.

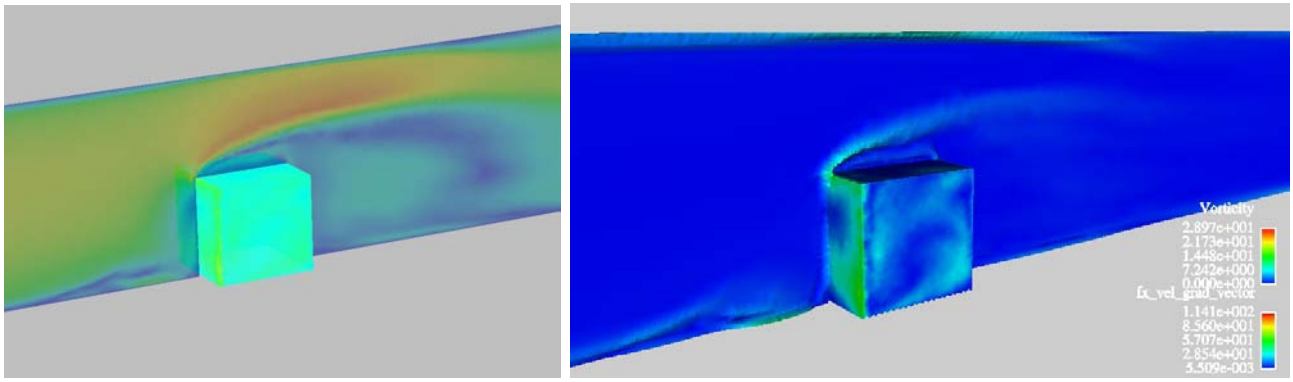


Figure 17: Left: Contour-fill velocity of the mean flow projected onto the center plane ($z = 0.0$). Right: Contour-fill vorticity of the mean flow projected onto the center plane ($z = 0.0$) and gradient velocity over cube.

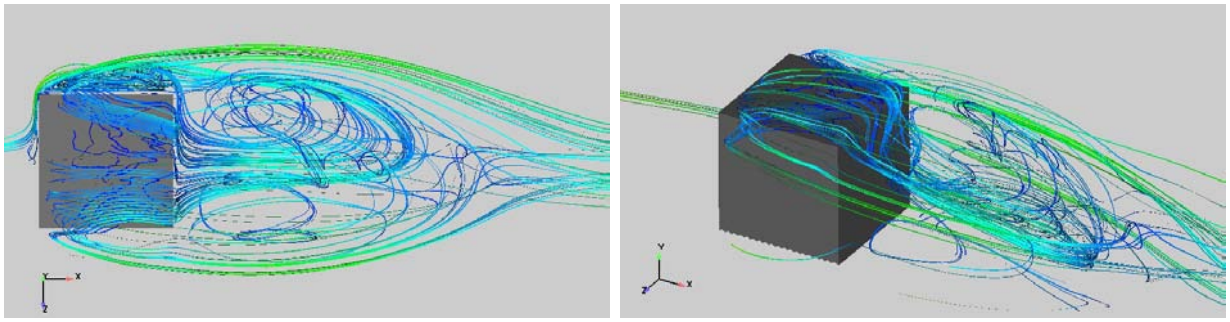

Figure 18: Exchange of the fluid between vortices in the time-averaged flow picture. Left: stream-ribbons (plant-view). Right: strectch of the stream-ribbons from the top to the backward vortices (perspective-view).

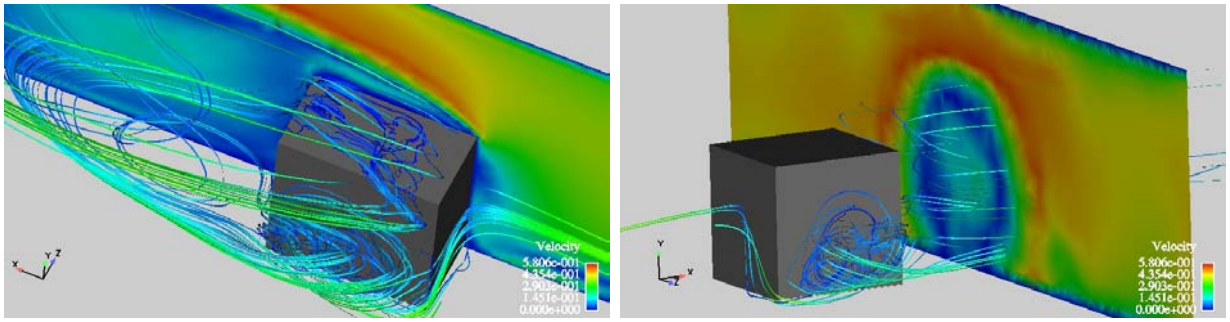


Figure 19: Exchange of the fluid between lateral and back vortices. Left: stream-ribbons time averaged velocity field and contour-fill $xy$-symmetric plane (flow direction right to left). Right: stream-ribbons and contour-fill $yz$-plane in near wake.

### 5.1.4 Trace-lines

In figure 20 time-averaged trace-lines are plotted on the body surface showing an unsteady flow in the front face and lateral sides. Can be observe a unsteady flow in top surface with a separation flow.

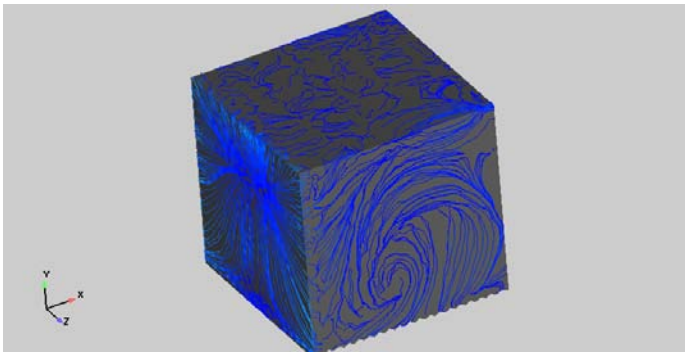

Figure 20: Trace-lines of the time-averaged flow over the body surrface.

### 5.1.5 Isosurfaces of the $Q$-criterion

For identifying coherent structures, a high vorticity modulus is a possible candidate, especially in free-shear flows, but the technique of iso-surfaces of the $Q$-criterion can be used to investigate the behaviour in transitional and turbulent flows. The so-called $Q$-criterion is another resource for studies of the coherent structures, which is often refered as a $\nabla\mathbf{u}$-based vortex "eduction method". It is based on both pressure and vorticity intensities, e.g. see Hunt *et al.*[21], and it can be defined as

$$Q = \frac{1}{2}\left(\Omega_{ij}\Omega_{ij} - S_{ij}S_{ij}\right) \ ; \tag{8}$$

where

$$\begin{aligned} \Omega_{ij} &= \frac{1}{2}\left(\frac{\partial u_i}{\partial x_j} - \frac{\partial u_j}{\partial x_i}\right) \ ; \\ S_{ij} &= \frac{1}{2}\left(\frac{\partial u_i}{\partial x_j} + \frac{\partial u_j}{\partial x_i}\right) \ ; \end{aligned} \tag{9}$$

are the symmetrical and skew-symmetrical components of the velocity gradient $\nabla\mathbf{u}$, respectively. In other words, the scalar $Q$ is the second invariant of the velocity gradient $\nabla\mathbf{u}$. From this definition it follows that:

- it is a balance between the squared rotation rate $\Omega^2 = \Omega_{ij}\Omega_{ij}$ and the strain rate $\epsilon(u) = S^2 = S_{ij}S_{ij}$;

- the isosurfaces with $Q > 0$ show sub-flows with rotation rates bigger than the strain ones, so they can develop coherent structures.

Since $\omega^2 = 2\Omega^2$, another equivalent definition is

$$Q = \frac{1}{4}\left(\omega^2 - 2S_{ij}S_{ij}\right) \ ; \tag{10}$$

showing that the coherent structures have a relatively high concentration of vorticity intensity $\omega$.

Figure 21 presents instantaneous isosurfaces of Q-criterion in a perspective view. This method is useful in identifying three-dimensional vortical structures. Several vortices and coherent structures (horseshoe, hairpin, and lateral vortices) are clearly identified. In particular, hairpin and lateral vortices evolve near wake downstream of the cubic obstacle.

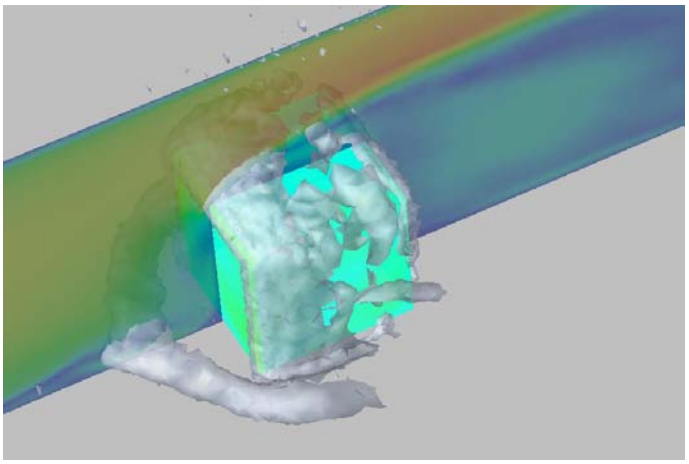

Figure 21: Instantaneous isosurface of the second invariant of the velocity gradient tensor (Q) $Q = 0.35$. Contour-fill velocity magnitude simmetric plane $z = 0.0$

Figure 22, at left, shows the isosurfaces $Q > 0$ for the mean flow with the magnitude scale cut off at the range $[0.1, 3.0]$, where a high vorticity fluctuation is observed in the top surface, lateral sides and near-wake. This picture shows a trumpet vortex and horseshoe vortex similar to the sketch above included in figure 3.

The same is observed with the threshold $[0.2, 0.5]$ in figure 22, right, where are visible a secondary corner vortex in front of the cube and it was possible to follow the lifespan of trumpet vortex from formation close to the front. Besides, it can be observed breakdown vortices in top surfaces and lateral sides.

## 6 CONCLUSIONS

The wall-mounted cube test was performed using CFD+LES(Smagorinsky) model. The methodology for computing the incoming velocity profile was explored chosing in this

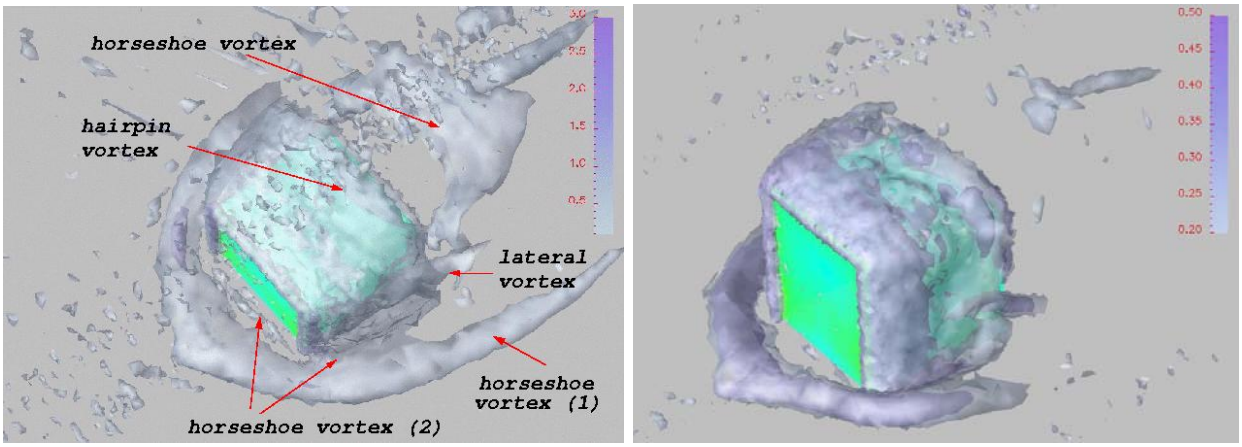


Figure 22: Iso-surfaces of the time-averaged $Q > 0$: threshold $[0.1, 3.0]$ (left) and $[0.2, 0.5]$(right).

work the resolution of an extra problem consisting of a turbulent developed channel flow. Results for the cube test show a general agreement with other published results. However more work should be done in order to obtain more accuracy in the results compared with another works published in similar conditions. After this validation task it is necessary to explore how to improve LES model, specially for replacing the constant Smagorinsky coefficient for another expression with more physical realism, or using an hybrid LES plus RANS for the subgrid scales, or appealing to multiscale mathematical formulation to get more information about the interaction of turbulence modeling and numerical stabilization terms. Other future work to do is using a posteriori flow statistics trying to understand how to improve the present results.

**Acknowledgments**

This work was partially performed with the *Free Software Foundation/GNU-Project* resources as `GNU/Linux OS` and `GNU/Octave`, as well another Open Source resources as `PETSc`, `MPICH` and `GiD`, and supported through grants CONICET-PIP-02552/2000, ANPCyT-FONCyT-PME-209 **Cluster**, ANPCyT-FONCyT-PID-99-74 **Flags**, and CAI+D-UNL-2000-43.

## REFERENCES

[1] Kogaki T., Kobayashi T., and Taniguchi N. Large eddy simulation of flow around a rectangular cylinder. *Fluid Dynamics Research*, **20**, 11–24 (1997).

[2] Rodi W., Ferziger J.H., Breuer M., and Pourquié M. Status of large-eddy simulation: result of a workshop. *ASME transactions*, **119**, 248–262 (June 1997).

[3] Storti M.A., Nigro N., M., and Paz R. Petsc-fem: A general purpose, parallel, multi-physics fem program.

[4] Sonzogni V.E., Yommi A., Nigro N., and Storti M. A parallel finite element program on a Beowulf Cluster. *Advances in Engineering Software*, **33**, 427–443 (2002).

[5] Krajnović S. and Davidson L. Large-eddy simulation of the flow around simplified car model. In *9th Int. Symp. of Flow Visualization*, pages paper 117, 1–10, (2000).
[6] Krajnović S. and Davidson L. Development of large-eddy simulation for vehicle aerodynamics. In *IMECE-ASME*, page paper 32833, New Orleands, (November 2002).
[7] Franck G., Nigro N., Storti M., and D'Elía J. Modelización del flujo del viento en el modelo de Ahmed. In *ENIEF 2003, XIII Cong. On Num. Meth.*, ISSN 1666-6070, pages 124–142, Bahía Blanca, Argentina, (November 4-7 2003).
[8] Franck G., Carazo F., Nigro N., Storti M., and D'Elía J. Numerical simulation of the flow around the Ahmed vehicle for a critical slant angle. In *ENIEF 2004, XIV Cong. On Num. Meth.*, pages 2189–2209, S.C. de Bariloche, Argentina, (November 8-11 2004).
[9] Filippini G., Franck G., Nigro N., Storti M., and D'Elía J. Large eddy simulations of the flow around a square-cylinder. In *Mecánica Computacional, vol. XXIV*, (November 08-11 2005).
[10] Smagorinsky J. General circulation experiments with the primitive equations: I. the basic equations. *Mon. Weather Rev.*, **91**, 99–164 (1963).
[11] Germano M., Piomelli U., Moin P., and Cabot W. A dynamic subgrid-scale eddy viscosity model. *Physics of Fluid*, **3**, 1760 (1991).
[12] Krajnović S. and Davidson L. A mixed one-equation subgrid model for large-eddy simulation. *Int. J. of Heat and Fluid Flow*, **23**, 413–425 (2002).
[13] Calo V.M. *Residual-based Multiscale Turbulence Modeling: finite volume simulations of bypass transition*. PhD thesis, Stanford University, (2005).
[14] D'Elía J., Franck G., Storti M., and Nigro N. Numerical simulations of a fully developed turbulent channel flow by finite elements. In *Mecánica Computacional, vol. XXIII*, pages 2047–2064, (November 08-11 2004).
[15] Dean R.G. and Dayrymple R.A. *Water Waves Mechanics for Engineers and Scientists*. Prentice-Hall, Englewood Cliffs, New Jersey, (1984).
[16] Deardorff J.W. A numerical study of three-dimensional turbulent channel flow at large reynolds numbers. *J. Fluid Mech.*, **41, Pt. 2**, 453–480 (1970).
[17] Kim J., Moin P., and Moser R. Turbulence statistics in fully developed turbulent channel flow at low Reynolds number. *Journal of Fluids Mechanics*, **177**, 133–166 (1987).
[18] Moin P. and Kim J. Numerical investigation of turbulent channel flow. *Journal of Fluids Mechanics*, **118**, 341–377 (1982).
[19] Hussein H. J. and Martinuzzi R. Energy balance for turbulent flow around a sueface mounted cube placed in a channel. *Physics of Fluids*, **A 8**, 764–780 (1996).
[20] Baker C.J. The laminar horseshoe vortex. *J. Fluid Mech*, **8**, 347 (1979).
[21] Hunt J.C.R., Wray A.A., and Moin P. Eddies, stream, and convergence zones in turbulent flows. *Report CTR-S88, Center For Turbulent Research*, (1988).